Article

Cell

Phosphatidylserine Vesicles Enable Efficient En Bloc Transmission of Enteroviruses

Graphical Abstract

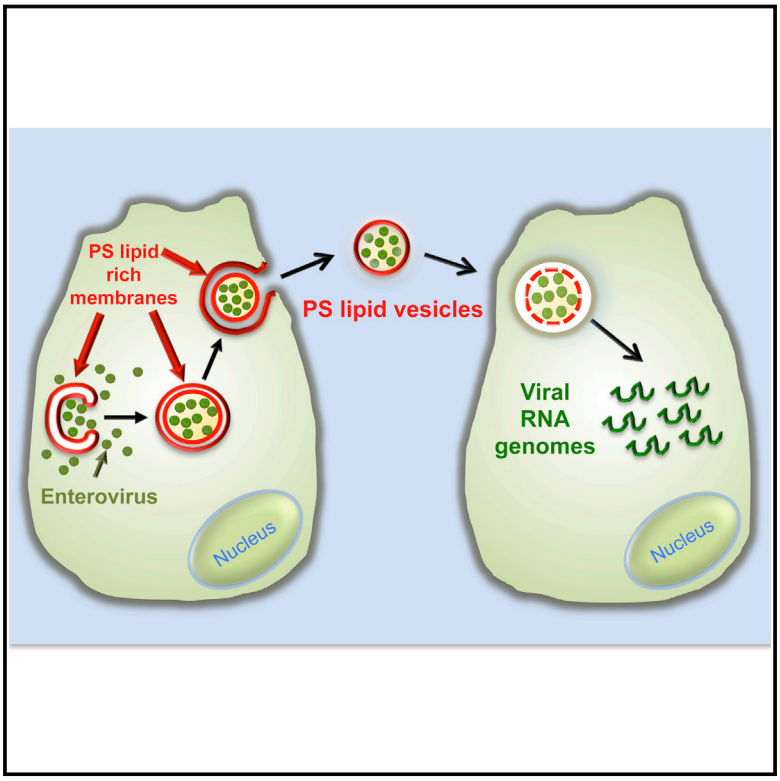

Authors

Ying-Han Chen, WenLi Du, ...,
Grégoire Altan-Bonnet,
Nihal Altan-Bonnet

Correspondence

nihal.altan-bonnet@nih.gov

In Brief

Clusters of enteroviruses are packaged in phosphatidylserine (PS)-enriched vesicles, thereby enhancing the infection efficiency of the viruses and enabling collective transmission of multiple viral genomes from cell-to-cell.

Highlights

- Clusters of viruses are packaged and released non-lytically in PS lipid vesicles
- PS lipids are co-factors in mediating subsequent infectivity and transmission
- PS vesicles provide greater infection efficiency for viruses
- PS vesicles enable viral genome clusters to be transmitted en bloc cell-to-cell

Chen et al., 2015, Cell *160*, 619–630
February 12, 2015
http://dx.doi.org/10.1016/j.cell.2015.01.032

CellPress

Cell

Phosphatidylserine Vesicles Enable Efficient En Bloc Transmission of Enteroviruses

Ying-Han Chen,[1,2] WenLi Du,[1] Marne C. Hagemeijer,[1] Peter M. Takvorian,[2] Cyrilla Pau,[2] Ann Cali,[2] Christine A. Brantner,[3] Erin S. Stempinski,[3] Patricia S. Connelly,[3] Hsin-Chieh Ma,[4] Ping Jiang,[4] Eckard Wimmer,[4] Grégoire Altan-Bonnet,[5] and Nihal Altan-Bonnet[1,*]

[1]Laboratory of Host-Pathogen Dynamics, National Heart Lung and Blood Institute, NIH, Bethesda, MD 20892, USA
[2]Federated Department of Biological Sciences, Rutgers University, Newark, NJ 07102, USA
[3]Electron Microscopy Core Facility, National Heart Lung and Blood Institute, NIH, Bethesda, MD 20892, USA
[4]Department of Molecular Genetics and Microbiology, Stony Brook University, Stony Brook, NY 11794, USA
[5]Program in Computational Biology and Immunology, Memorial Sloan Kettering Cancer Center, New York, NY 10065, USA
*Correspondence: nihal.altan-bonnet@nih.gov
http://dx.doi.org/10.1016/j.cell.2015.01.032

SUMMARY

A central paradigm within virology is that each viral particle largely behaves as an independent infectious unit. Here, we demonstrate that clusters of enteroviral particles are packaged within phosphatidylserine (PS) lipid-enriched vesicles that are non-lytically released from cells and provide greater infection efficiency than free single viral particles. We show that vesicular PS lipids are co-factors to the relevant enterovirus receptors in mediating subsequent infectivity and transmission, in particular to primary human macrophages. We demonstrate that clustered packaging of viral particles within vesicles enables multiple viral RNA genomes to be collectively transferred into single cells. This study reveals a novel mode of viral transmission, where enteroviral genomes are transmitted from cell-to-cell en bloc in membrane-bound PS vesicles instead of as single independent genomes. This has implications for facilitating genetic cooperativity among viral quasispecies as well as enhancing viral replication.

INTRODUCTION

Enteroviruses are a large genus of single positive-stranded RNA viruses whose members including poliovirus (PV), Coxsackievirus, rhinovirus, and enterovirus 68 are the causative agents of a number of important and widespread human diseases including poliomyelitis, myocarditis, hand foot and mouth disease, the common cold, and more recently, a severe respiratory disease with paralytic symptoms. In addition to >70 enteroviral serotypes identified in humans, enteroviral quasispecies are common largely as a result of inherent error making and lack of proofreading mechanisms of viral RNA-dependent RNA polymerases (RdRp).

Enteroviral RNA genomes serve as templates for both translation and replication, and these processes take place on host intracellular membranes (den Boon and Ahlquist, 2010; Hsu et al., 2010). After enteroviruses have bound their specific host receptors either at the cell surface or within endocytic vesicles (Brandenburg et al., 2007), the capsid undergoes a conformational change that allows the viral RNA to be transferred across the plasma membrane and/or endosomal membrane into the cytoplasm through a yet completely defined mechanism (Strauss et al., 2013). In the cytoplasm, the enteroviral RNA is first translated into non-structural proteins and structural proteins, where the former makes up the RNA genome replication machinery and the latter the capsid. The viral RNA replication machinery are then assembled on the cytoplasmic membrane leaflet of ER-derived membranes that are subsequently modified by viral and host proteins to have a specific lipid blueprint of enrichment in phosphatidylinositol-4-phosphate (PI4P) and cholesterol lipids. These lipids regulate the membrane association, assembly, and activity of the viral replication protein complex, including the RdRp, and thus facilitate viral RNA synthesis (Hsu et al., 2010; Ilnytska et al., 2013; Nchoutmboube et al., 2013).

Once the enteroviral RNA is synthesized, little is known about where in the host cell it is packaged in capsids and how these capsids are released from cells. While enteroviruses have historically been considered non-enveloped (i.e., lacking a host-derived membrane bilayer around their capsids) and thus rely on cell lysis to exit, recent reports of extracellular Coxsackievirus B3 (CVB3) being present in vesicles (Robinson et al., 2014) and PV being able to spread non-lytically among host cells (Bird et al., 2014) have raised important questions regarding the extracellular nature of enteroviral particles and the significance of non-lytic exit in the viral life cycle. Moreover hepatitis A, hepatitis E and blue tongue viral particles, all long considered non-enveloped, have been observed surrounded by membranes (Feng et al., 2013; Takahashi et al., 2008; Owens et al., 2004).

A central paradigm in virology is that viruses behave as independent infectious units (Flint et al., 2009). While there are exceptions to this, such as vaccinia virus particles preventing superinfection by inducing the host cell to repel other virions (Doceul et al., 2010), it is largely accepted that the fate of individual viral genomes are not dependent on one another during exit from one cell and entry into another (Brandenburg and Zhuang

2007). Here, we investigate the assembly, exit, and subsequent infection processes of enteroviral particles using a combination of imaging techniques including confocal microscopy, super-resolution light microscopy, correlative light, and electron microscopy along with single molecule RNA fluorescence in situ hybridization (FISH), proteomic, and biochemical approaches. We show that multiple infectious enteroviral particles are clustered within individual phosphatidylserine (PS) lipid-enriched vesicles and non-lytically secreted out of cells. These viral particles in vesicles are more efficient in establishing infection than free viral particles. We demonstrate that vesicles encapsulate and traffic large numbers of mature infectious viral particles between cells and consequently enable the transfer of multiple viral RNA genomes collectively into new host cells by a mechanism that is dependent on both the virus-specific receptor of the recipient host cell as well as the vesicular PS lipids.

RESULTS

Assembled Poliovirus Capsids Are Localized to Viral RNA Replication Organelles

We first investigated the intracellular spatio-temporal dynamics of newly synthesized PV particles. The generation of PV particles, as well as enterovirus assembly in general, comprises a multistep process where capsid subunits (VP0, VP1, VP3) form pentamers, which polymerize into capsids (Liu et al., 2010). Once RNA is packaged, the VP0 subunits get cleaved into VP2 and VP4 to generate mature infectious virions (Liu et al., 2010). From screening a large number of neutralizing antibodies, we identified the A12 antibody, that binds deep inside the canyon bridging both rims of two adjacent pentamers and thus recognizing assembled capsids (Chen et al., 2011, 2013), to visualize PV capsids within infected cells. We fixed cells at various intervals after PV infection and co-immunolabeled with A12, anti-viral VP1 to detect individual VP1 subunits, and anti-viral 3AB antibodies, the latter to detect viral 3AB to localize replication organelles where viral RNA is synthesized (Hsu et al., 2010). Newly assembled capsids were clearly detectable from 3–4 hr post-infection (p.i.) and onward, and they were localized to the replication organelles (Figure 1A). Note that in contrast to A12 labeling, VP1 was localized to both the replication organelles and dispersed across the cytoplasm, consistent with its cytosolic nature. At 6–7 hr p.i., capsids were dispersed from the replication sites to the cytoplasm and sequestered in puncta (Figure 1A, 6–7 hr p.i. inset). At this time, there is a known cessation in viral RNA synthesis (Ehrenfeld et al., 1970), and the timing of capsid release from replication organelles was coupled to viral RNA synthesis since prematurely inhibiting viral RNA synthesis with the inhibitor Guanidine HCl (Barton and Flanegan, 1997) triggered capsids to rapidly disperse into the cytoplasm (Figure S1A).

Poliovirus Capsids Are Captured by Phosphatidylserine Lipid-Enriched Autophagosome-like Organelles and Released Non-Lytically from Cells

Between 6 and 7 hr p.i., we found that >85% of capsids (n = 10 cells) were on punctate cytoplasmic structures that colocalized with the autophagosomal membrane protein, LC3-II (Figure 1B). By transmission electron microscopy, we observed numerous double-membraned autophagosome-like organelles containing capsids (Figure 1C). Previous reports (Taylor et al., 2009; Kirkegaard and Jackson, 2005; Jackson et al., 2005) had found that perturbation of the host autophagy pathway led to a decrease in PV release from infected cells. Consistent with that, either disrupting autophagy by small interfering RNA (siRNA) depletion of autophagy machinery LC3 or beclin 1, or acutely stimulating autophagy by treating cells with tat-beclin 1 peptides, blocked or enhanced PV release by ~10-fold, respectively (Figures S1B and S1C) while replication was unaffected (Figure S1D). However, these capsid containing autophagosome-like organelles did not follow the conventional autophagy pathway and fuse their contents with lysosomes as inhibiting lysosomal enzymes did not further increase LC3-II levels beyond the 4-fold increase observed in PV-infected cells (Figures S1E and S1F) and none of the A12/LC3-II co-labeled structures contained lysosomal enzymes at any point during infection (Figures S1F and S1G). Notably, the SNARE protein syntaxin 17, normally localized to autophagosomes and required for fusion with lysosomes (Itakura et al., 2012), did not localize to these A12/LC3-II co-labeled structures (Figure S1I).

However, we found that the membranes of both the replication organelles and the autophagosome-like organelles contained negatively charged phosphatidylserine (PS) lipids. PS lipids in uninfected cells are primarily located at the cytoplasmic leaflets of the plasma and endosomal membranes as well as at the lumenal leaflet of the ER membrane (Leventis and Grinstein, 2010; Kay et al., 2012). Cells were co-transfected with GFP-LactC2 and FAPP1mRFP, cytosolic live-cell reporters for PS (Kay et al., 2012), and PI4P lipids, respectively, the latter to report on the location of the ER-derived replication organelle membranes (Hsu et al., 2010). At 4 hr p.i., cells were imaged live by structured illumination microscopy. Highly localized PS-rich membrane domains exposed to the cytoplasm were found distributed across the replication organelles (Figure 1D, inset). Later, between 6 and 7 hr p.i., cells were fixed and immunolabeled with anti-GFP and A12 antibodies and imaged by confocal microscopy. Numerous A12 positive structures were found also co-labeled with GFP-LactC2 indicating the presence of PS lipids on their membrane leaflets exposed to the cytoplasm (Figure 1E, arrows). Consistent with this, in PV-infected live cells co-expressing LC3-mRFP and GFP-LactC2, >90% (organelles measured across ten cells) of the LC3-mRFP-labeled autophagosome-like organelles were co-labeled with GFP-LactC2 (Figure 1F, inset).

We then investigated the fate of these capsid-containing organelles during the rest of the infection time period. Between 7 hr and 8 hr p.i., there was a 70% ± 10% (n = 15) decrease in the number of capsids within the cytoplasm (Figure 1G). Using the cell impermeable Trypan blue dye, we found that the plasma membrane remained intact during this time while there was an ~6-fold increase in extracellular viral titers (Figure 1H). This lack of plasma membrane permeability during PV infection had also been previously observed (Taylor et al., 2009; Bird et al., 2014). Although by 12 hr p.i. the cells eventually lysed (not shown), this data indicated that the majority of PV particles were released prior to cell lysis.

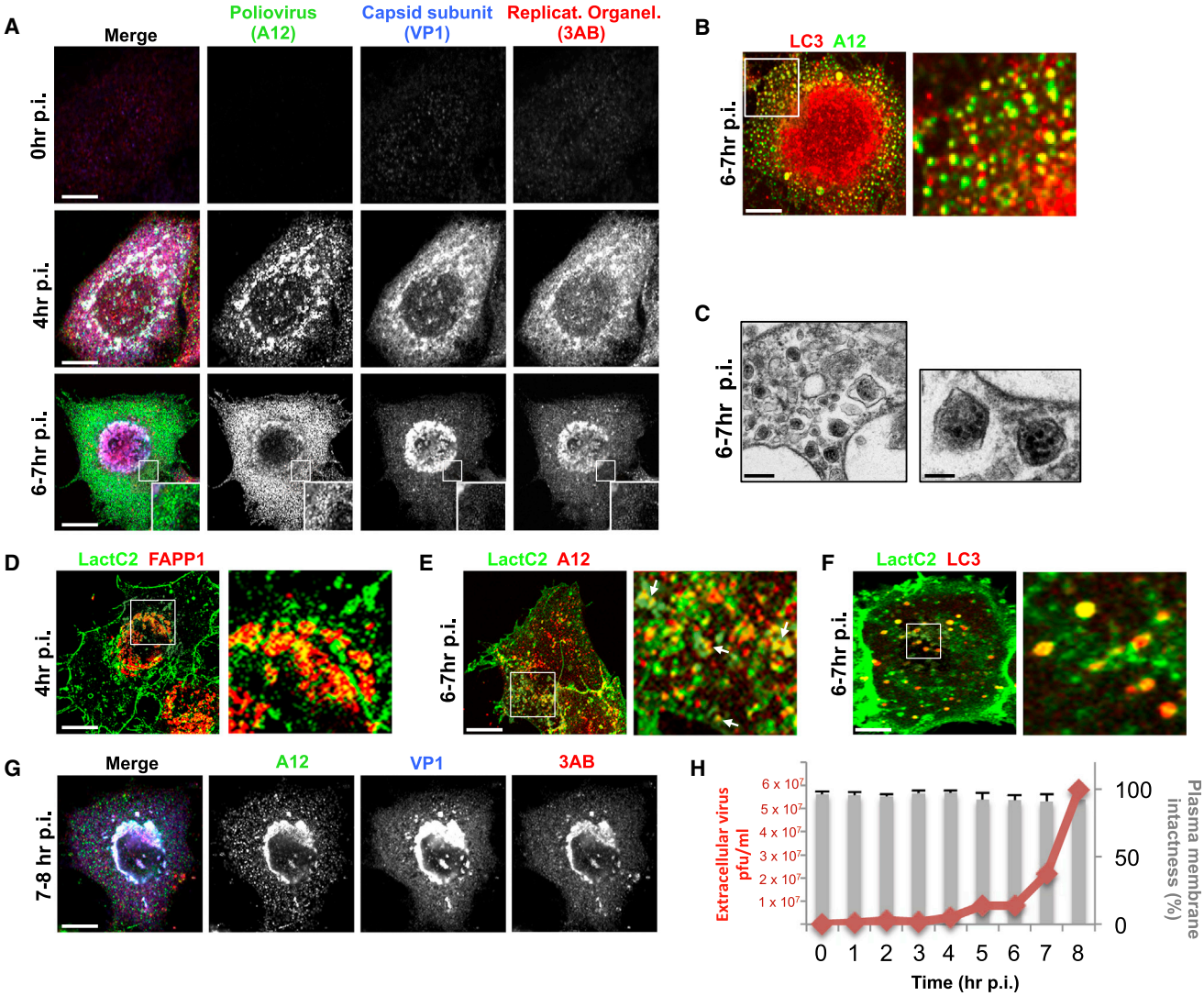

Figure 1. Poliovirus Capsids Are Captured by Phosphatidylserine Lipid-Enriched Autophagosome-like Organelles and Released Non-Lytically from Cells

(A) Capsids undergo dynamic spatial transitions during infection. HeLa cells infected with PV and immunolabeled with A12, anti-VP1, and anti-3AB antibodies. Scale bars represent 5 μm.

(B) Capsids (A12) colocalized with autophagosome marker LC3-II. PV-infected HeLa cells were immunolabeled with A12 and anti-LC3-II antibodies. Scale bar represents 5 μm.

(C) Electron micrographs of PV-infected cells show PV capsids in double-membrane autophagosome-like organelles. Scale bars represent 5 μm and 200 nm (inset).

(D) PV-infected cells at 4 hr p.i. expressing GFP-LactC2 and FAPP1mRFP imaged by structured illumination microscopy. Region of interest is magnified in right panel. Scale bar represents 5 μm.

(E) PV-infected cells at 7 hr p.i. expressing GFP-LactC2 were immunolabeled with anti-GFP and A12 antibodies. Region of interest is magnified in right panel. Arrows indicate A12 positive autophagosome-like organelles co-labeled with GFP-LactC2. Scale bar represents 5 μm.

(F) Cells co-expressing GFP-LactC2 and LC3-RFP were infected with PV and imaged by confocal microscopy at 7 hr pi. Region of interest is magnified in right panel. Scale bar represents 5 μm.

(G) Capsid distribution between 7 and 8 hr p.i. PV-infected cells were immunolabeled with A12, anti-VP1, and anti-3AB antibodies. Scale bar represents 5 μm.

(H) Plasma membrane integrity remains intact when PV exits cells. Trypan Blue diffusion across the plasma membrane was measured concurrently with measurements of extracellular PV titer, the latter plotted in plaque-forming units/ml (pfu/ml).

See also Figure S1.

Extracellular PV Particles Are Found in Uniformly Large Vesicles

Scanning electron microscopy (SEM) of cells at 7 hr p.i. cells revealed numerous vesicular structures of similar size docked at the extracellular side of the intact plasma membrane (Figure 2A and inset). While these SEM images may not reflect the true shape and size of these vesicles within live cells, they do point to a striking uniformity in size. Measurements of the cross-section

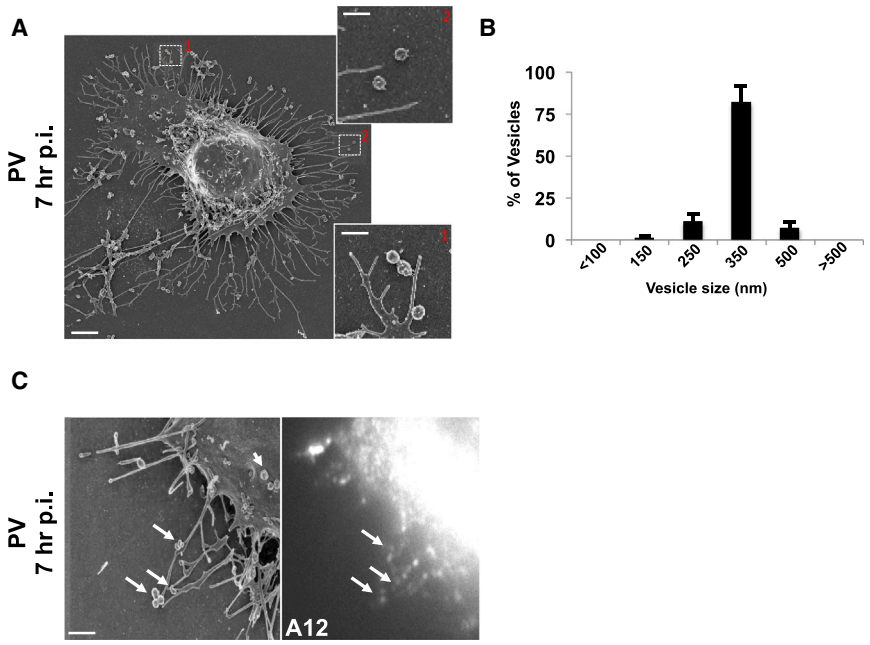

Figure 2. Extracellular PV Particles Are Found in Large Uniform-Sized Vesicles

(A) Scanning electron microscopy of a PV-infected cell at 7 hr p.i. Scale bar represents 3 μm. Inset shows higher magnification of uniform size vesicles docked on the extracellular side of the plasma membrane. Scale bar represents 1 μm.

(B) Extracellular vesicle size distribution in PV-infected cells. Cross section diameter of a 100 randomly selected extracellular vesicles from four different cells, were measured from scanning electron micrographs and plotted. Data represented as mean ± SEM.

(C) Correlative fluorescence and scanning electron microscopy (SEM). PV-infected cell was immunolabeled with A12 at 7 hr pi, epifluorescence image was obtained (right) and then sample was processed for SEM (left). Arrows point to A12-labeled extracellular vesicles. Scale bar represents 1 μm.

diameter from 100 randomly selected extracellular vesicles from four different cells, showed that ~90% of the vesicles were between 250 nm and 350 nm in diameter (Figure 2B). Correlative fluorescence imaging in conjunction with SEM confirmed that these vesicles contained A12-labeled capsids (Figure 2C).

Mature Enteroviral Particles Are Released in PS-Enriched Vesicles

We next investigated whether the extracellular vesicles containing PV retained the PS lipids that had been components of the autophagosome-like organelles (Figures 1D and 1F). Incubation of PV-infected cells with Alexa 568 coupled Annexin V, a non-cell permeable fluorescent reporter protein for PS lipids (Koopman et al., 1994), revealed numerous fluorescent puncta dotting the surface of the cell at 7hr p.i. (Figure 3A). Similar results were also observed with CVB3 (at 7 hr p.i.) and human rhinovirus infections (at 12 hr p.i.) (Figure 3A). Note that this pattern of Annexin V labeling of enterovirus-infected cells was different from both apoptotic- and mock-infected cells: in the former, the entire plasma membrane was labeled with Annexin V as a result of PS lipids being on the extracellular membrane leaflet of the cell, a hallmark of apoptosis (Figure 3B, apoptosis) while in the latter there was no labeling since PS lipids were on the cytosolic leaflet of the plasma membrane (Figure 3B, mock).

We performed time-lapse confocal/differential interference contrast (DIC) imaging on PV-infected cells in the presence of Alexa 568-Annexin V to determine if these vesicles were being released. We observed Annexin V-labeled vesicles emerging from the cell surface at discrete domains and being rapidly released into the extracellular medium (Figure 3C; arrow; Movie S1). We then quantified the amount of PS vesicles released during PV, CVB3, or rhinovirus infection relative to mock-infected cells (for each respective virus). We collected the extracellular medium, removed large cell debris, and enriched for vesicles of size range 100–500 nm using differential centrifugation. This size range was chosen based on our previous light and electron microscopy data (Figure 2). The enrichment for vesicles of this size range was confirmed by transmission electron microscopy (Figure S2A). The vesicles were incubated with Alexa 568-Annexin V, and following the wash to remove any unbound Annexin V, placed in a spectrofluorometer. Fluorescence measurements revealed a net ~9-fold, ~3-fold, and ~3-fold increase in amounts of PS vesicles collected from the supernatants of PV-, CVB3-, and rhinovirus-infected cells, respectively, compared to mock-infected cells (Figure 3D).

We subsequently enriched for PS vesicles from the collected vesicle fraction using magnetic separation with Annexin V-conjugated magnetic microbeads. In parallel, vesicles were also incubated with magnetic microbeads lacking Annexin V to control for nonspecific binding. Post-magnetic separation, the samples were processed for SDS-PAGE/western analysis. We found that the extracellular vesicles both pre- and post-Annexin V isolation, had a VP2/VP0 ratio ~2-fold greater than the whole cell lysate (Figure 3E). This indicated that these extracellular released PS vesicles were not non-specific shedding of host membrane but rather conduits for the selective release of mature PV particles. Similar results were also obtained from human rhinovirus 2-infected cells where PS vesicles were found to contain mature viral particles (Figure 3F).

Infection by PV Particles in Vesicles Is Dependent on Both the Virus-Specific Receptor and the PS Lipids

We next compared the infection capability of PV particles within vesicles released from cells compared to free viral particles. Free viral particles were obtained by three cycles of quick freeze-thaw of the vesicle fraction. Freeze-thaw does not significantly impact PV infectivity (Strazynski et al., 2002), and no difference in infectivity was observed by plaque assay between equivalent numbers of PV particles isolated by freeze thaw or collection from the supernatant of post-vesicle enrichment fractions (data

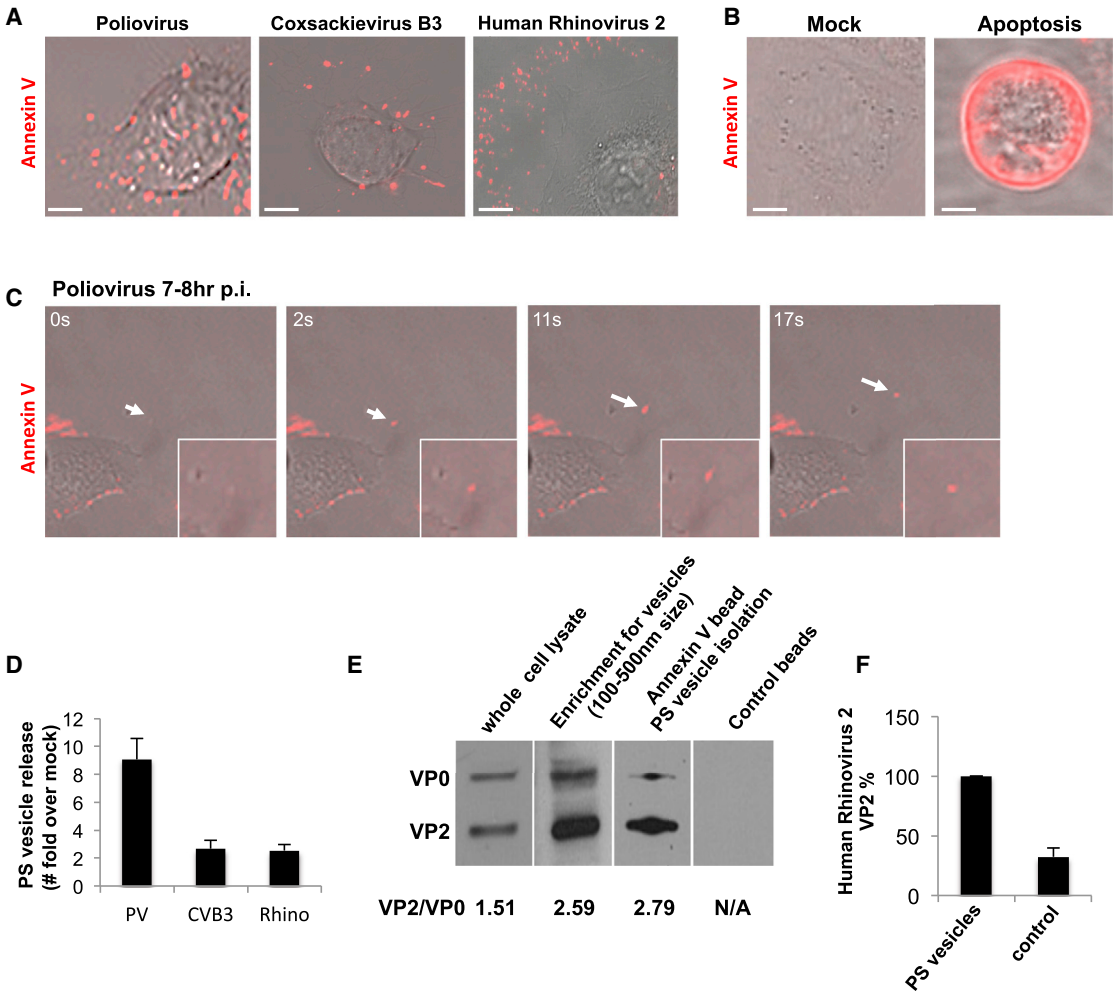

Figure 3. Mature PV, CVB3, and Rhinovirus Particles Are Released in Phosphatidylserine Lipid Vesicles

(A) Cells infected with PV, CVB3, or rhinovirus were incubated with Alexa 568-Annexin V and imaged by confocal/DIC microscopy at 7 hr p.i. Scale bar represents 5 μm for PV and rhinovirus, 10 μm for CVB3.

(B) Mock and apoptotic HeLa cells labeled with Alexa 568-Annexin V and imaged by confocal/DIC microscopy. Scale bar represents 10 μm.

(C) Dynamics of Alexa 568-Annexin V-labeled PS vesicle release from plasma membrane projections of PV-infected cells at 7 hr p.i.

(D) Quantification of PS vesicles released from enterovirus-infected cells.

(E) VP2/VP0 ratio of whole cell lysate and PS vesicles in PV-infected cells. Annexin V-isolated PS vesicles from PV-infected cells at 7 hr p.i. were analyzed by SDS-PAGE/western with anti-PV VP2 antibody.

(F) PS vesicles from human rhinovirus-infected cells contain mature rhinoviral particles. Isolated PS vesicles were processed for SDS-PAGE/western analysis with anti-HRV2/VP2 (neutralizing) antibodies.

See also Figure S2 and Movie S1.

not shown). The collected extracellular vesicles from PV-infected cells or free PV particles were then incubated with a confluent layer of HeLa cells (Figure 4A). After 4 hr of infection with either vesicles or free viral particles, numerous PV-replicating (based on immunofluorescence labeling of VP1) infected cells were found in both cell populations (Figure 4A).

To determine if the PV particles within vesicles still required the PV receptor CD155 on the host cell for infection, cells were incubated with CD155 neutralizing antibodies prior to exposure to vesicles and viral 3AB replication protein levels were measured after 4 hr of infection. In the presence of neutralizing antibodies, vesicle infectivity was inhibited by >95% indicating that PV vesicles were not just simply "fusing" with cells but that the viral particles within the vesicles still required binding to PV receptor for transfer of viral RNA into the host cell cytoplasm (Figure 4B).

We next determined if the infection was dependent on PS lipids of the vesicles. Vesicles isolated by differential centrifugation were incubated with different amounts of Annexin V protein, which binds and masks the PS head-groups on the lipids (Swairjo et al., 1995). After removing any unbound Annexin V, the vesicles were added to HeLa cells and replication measured after 4 hr. Strikingly, masking of the vesicle-associated PS lipids by Annexin V, inhibited PV infection of the host cells in a dose-dependent manner (Figures 4C and 4D). These data indicated

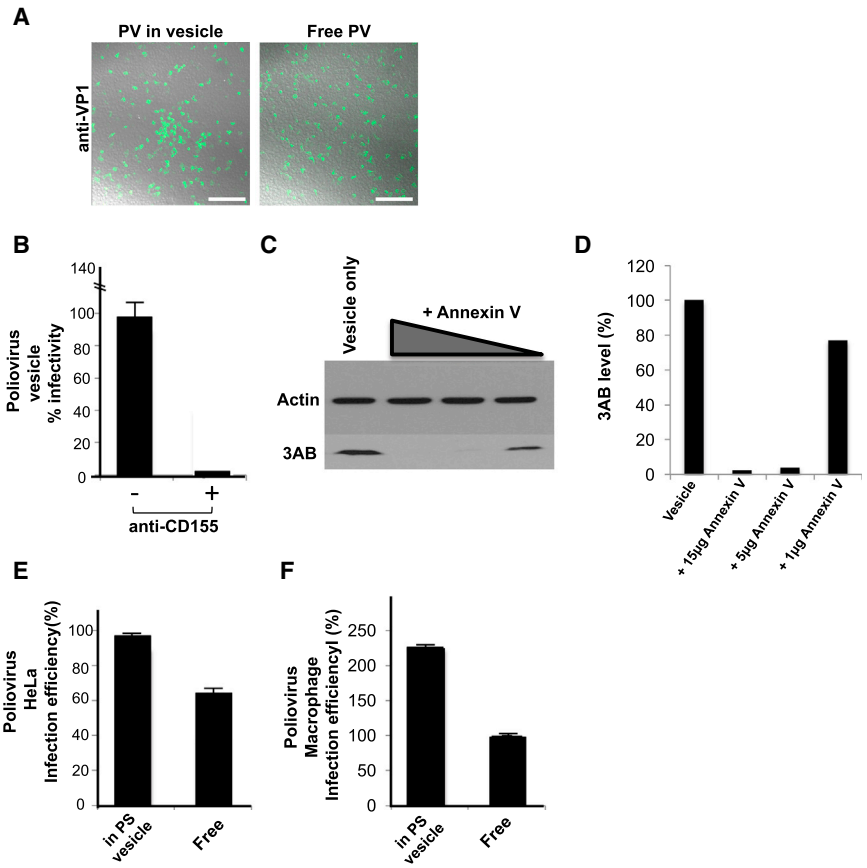

Figure 4. Infection by PV Particles in Vesicles Is More Efficient Than Free Viral Particles and Is Dependent on Both the Poliovirus Receptor and PS Lipids

(A) Free or vesicle-associated PV particles were incubated with new recipient cells and replication was detected at 4 hr p.i. by immunolabeling with anti-VP1 antibodies. Scale bar represents 500 μm.

(B) CD155/PVR neutralizing antibodies block infection PV particles in vesicles.

(C) Blocking PS lipids on vesicles containing PV particles block infection. Vesicles collected by differential centrifugation were incubated with different amounts of Annexin V protein prior to incubation with recipient HeLa cells. Replication was measured at 4 hr p.i., by SDS-PAGE/western analysis with anti-3AB antibody.

(D) Quantification of western results in (C).

(E) HeLa cells were incubated with equal titers of free and vesicle-associated PV particles. Infection efficiency was determined by quantifying viral 3AB protein levels at peak replication time (4 hr p.i.). Data represented as mean ± SD.

(F) Primary human macrophages were incubated with equal titers of free and vesicle-associated PV particles. Infection efficiency was determined by quantifying viral 3AB protein levels at peak replication time (8 hr p.i.). Data represented as mean ± SD.

that PS lipids are cofactors for PV infection and that mature infectious PV particles are predominantly in the PS vesicle fraction of vesicles collected by differential centrifugation.

Infection by PV Particles in Vesicles Is More Efficient Than Free PV Particles

We next measured and compared the level of infection of host cells when infected with equivalent numbers of PV particles either in vesicles or as free. As a measure of infection efficiency, we quantified and plotted the levels of viral 3AB replication proteins at peak replication times (Figures 4E and 4F). Due to viral RNA synthesis feeding back on viral RNA translation (and vice versa), 3AB levels reflect viral RNA levels (Hsu et al., 2010). We found that at 4 hr p.i. of HeLa cells, viral 3AB levels were ~40% greater in cells incubated with PV particles in vesicles than free PV particles (Figure 4E). This difference was even more striking when primary human macrophages, cells that are specialized to recognize and take up PS lipid-containing cells and vesicles (Fadok et al., 1992), were used as the recipient host. Here vesicle-enclosed PV particles were almost 2-fold greater in infection efficiency compared to free PV particles (Figure 4F).

Unilamellar PS Vesicles Released from PV-Infected Cells Contain Multiple Viral Particles

To quantify the clustering of viral particles within vesicles, we collected free and vesicle-associated PV particles and immunolabeled them with A12 antibodies. We then imaged the cover-glass-immobilized PV particles by total-internal reflection fluorescence (TIRF) and by DIC microscopy (Figure 5A). Viruses were deposited on coverslip in two formats: vesicle-free fraction ("Free"), or vesicle-embedded fraction ("Vesicular"). Imaging revealed cluster of viruses within vesicles, while free viruses yielded a more diffuse distribution (Figure 5A). We quantified the difference in distribution of measured fluorescence by computing the radial autocorrelation functions $g(r)$ for the intensity map $I(\vec{u})$:

$$g(r) = \left\langle \oint_{\|\vec{v}\|=r} I(\vec{u}) I(\vec{u}+\vec{v}) d\vec{u} \right\rangle_{\vec{u}}.$$

The observed exponential decay of these autocorrelation functions enabled us to quantify the length scales that characterize the imaged aggregates (Figure 5B). We found that vesicle-embedded viruses yielded a characteristic clustering scale of 2.0 ± 0.1 μm (n = 4 images), while free virus yielded a five-time smaller characteristic scale of 0.4 ± 0.1 μm (n = 2 images). However, these estimates are too close to the spatial resolution of TIRF imaging and thus only qualitative. To circumvent this diffraction limit, we then applied the direct stochastic optical reconstruction microscopy (dSTORM) methodology to achieve super-resolution of these viral particles (Figure 5C). dSTORM relies on sequential imaging and fitting to achieve a spatial resolution of individual dyes within 30 nm (Bates et al., 2007; Baddeley et al., 2009; Dempsey et al., 2011).

In order to assess the degree of clustering within these viral spreads we used the Ripley's K statistical test. By definition,

$$K(r) = \frac{A}{n^2}\sum_{i \neq j}\delta(d_{ij}/r),\ with\ \delta(x) = \begin{cases} 1\ for\ x \leq 1 \\ 0\ for\ x > 0 \end{cases},$$

with d_{ij} being the distance between the i^{th} and j^{th} points, A is the image area. By definition, $K(r)/\pi r^2$ is around 1 for a homogenous distribution of points, and larger than 1 for clustered spatial distribution (Veatch et al., 2012; Termini et al., 2014). Based on the electron microscopy images (Figures 2A, 2B, and S2A), we anticipated clusters of viruses within vesicles of 200—400 nm diameter. Hence, we calculated $K(r = 200\ nm)$ from the dSTORM data to test whether vesicles contained clusters of viruses: we found that $K(r = 200\ nm) = 2.4 \pm 0.9$ for free viruses and $K(r = 200\ nm) = 13.7 \pm 6.7$ for viruses within vesicles (Figure 5D). Hence, super-resolution microscopy does confirm that these viral vesicles do pack large numbers of viruses.

Consistent with these findings, transmission electron micrographs of PS vesicles (after isolation by Annexin V-coupled microbeads) revealed multiple clustered viral particles surrounded by a single membrane bilayer (Figure 5E). Per 200 nm cross-section, a single vesicle contained on average 19 ± 3 PV particles (n = 6 vesicles).

The presence of a single bilayer, as opposed to multiple bilayers, also indicated that the double-membraned autophagosome-like organelles had fused with the plasma membrane, rather than budded, in order to release PS vesicles. Thus, the PS lipids on the extracellular membrane leaflet of the vesicle are in a compartment that is topologically equivalent to the lumenal membrane leaflet of the double-membraned autophagosome-like organelle. The ER is a major membrane source for autophagosomes (Hamasaki et al., 2013) and has lumenal membrane leaflet enriched in PS lipids (Kay et al., 2012). Given that the isolated PS vesicles also contain ER-resident proteins (Figure S2B), it is highly likely that the autophagosome-like organelles, and thereby the released PS vesicles, originated from ER and/or ER-derived replication organelle membranes.

Vesicles Allow Multiple Viral RNA Molecules to Be Collectively Transferred into Cells

Given our dSTORM and TEM finding, we conjectured that multiple PV particles within a single vesicle might allow multiple viral genomes to be simultaneously transferred into a single cell. To test this hypothesis, we performed single molecule fluorescence in situ hybridization (single molecule RNA FISH) (Raj et al., 2008). Multiple oligonucleotide fluorescent probes hybridizing to an RNA molecule allow sufficient sensitivity to detect single RNA molecules within cells (Shaffer et al., 2013; Lubeck and Cai 2012).

Forty-eight fluorescently labeled nucleic acid probes, each 22 nucleotides in length, complementary to the PV genome, were synthesized. Fixed numbers of HeLa cells were incubated with different titers of either free PV particles or vesicle-associated PV particles for 1.5 hr and processed for FISH labeling as described previously (Shaffer et al., 2013) (Figure 5F). Note that we could exclude the possibility of any viral RNA synthesis occurring during this incubation time because cells with and without Guanidine HCL, an inhibitor of viral RNA synthesis, showed similar amounts of viral RNA molecules per cell (Figures 5G and S3).

For cells incubated with free PV particles, discrete fluorescent puncta, spatially segregated from one another in the cytoplasm were detected in individual cells (Figure 5F, free virus). In contrast for cells incubated with equivalent titers of PV particles in vesicles, there were many more fluorescent puncta, spatially juxtaposed (Figure 5F, virus in vesicle). The lowest multiplicity of infection with free viral particles was observed at 1.5×10^7 pfu/ml where there was on average only one fluorescent puncta per cell (Figures 5F and 5H, free virus). Hence, the size of these puncta was approximated as a single viral RNA molecule and used in subsequent quantification and analysis of FISH data. At each titer, for either free virus or vesicle-associated virus, 55 cells were randomly chosen and viral RNA molecules counted in each cell. The number of viral RNA molecules per cell were subsequently plotted in Figure 5H.

From our quantification, we found that at 12×10^7 pfu/ml and 6×10^7 pfu/ml, there were ~40% and ~75%, respectively, more viral RNA molecules per cell when PV particles were presented in vesicles than as free virus (Figure 5H). Indeed, for cells incubated with free PV particles, we found that as the viral titer decreased 4-fold (from 12×10^7 pfu/ml to 3×10^7 pfu/ml), there was a ~90% decrease in the number of PV RNA molecules per cell whereas for cells incubated with PV particles in vesicles, this decrease was significantly less, only ~40% (Figure 5H). Furthermore, at any given titer there were significantly more cells with >15 PV RNA molecules within them when they had been infected with PV in vesicles as opposed to free PV (Figure 5I). These data are consistent with our dSTORM findings (Figures 5A–5D) and transmission electron micrographs of isolated PS vesicles (Figure 5E) and indicate that vesicles contain multiple PV particles, which enable multiple viral RNA genomes to be transferred en bloc into a cell. Note that there was a large variation in the number of viral RNA genomes per cell when cells were infected with PV particles in vesicles as opposed to free PV particles (Figures 5H and 5I). Since de novo viral RNA synthesis can be ruled out, this variation is likely due to differences in the number of viral particles packaged per vesicle as well as contamination from free particles due to possible vesicle lysis.

DISCUSSION

Here, we have shown that multiple mature infectious enteroviral particles are released in single unilamellar PS lipid vesicles, which in turn enables multiple viral genomes to be collectively transferred to an individual cell in a new round of infection. These PS vesicles containing multiple viral genomes appear to be significantly more efficient in infection and may facilitate genetic cooperation among viral genomes.

We first detected assembled PV capsids at replication organelles where viral RNA was synthesized (Figures 1A and 6). This close juxtaposition of capsids with viral RNA synthesis sites would serve to immediately encapsidate the viral RNA and thereby facilitate efficient genome packaging as well as protection of viral genomes from host defenses. These viral particles then translocated into the cytoplasm, which was not only temporally coincident with a cessation of viral RNA synthesis but also

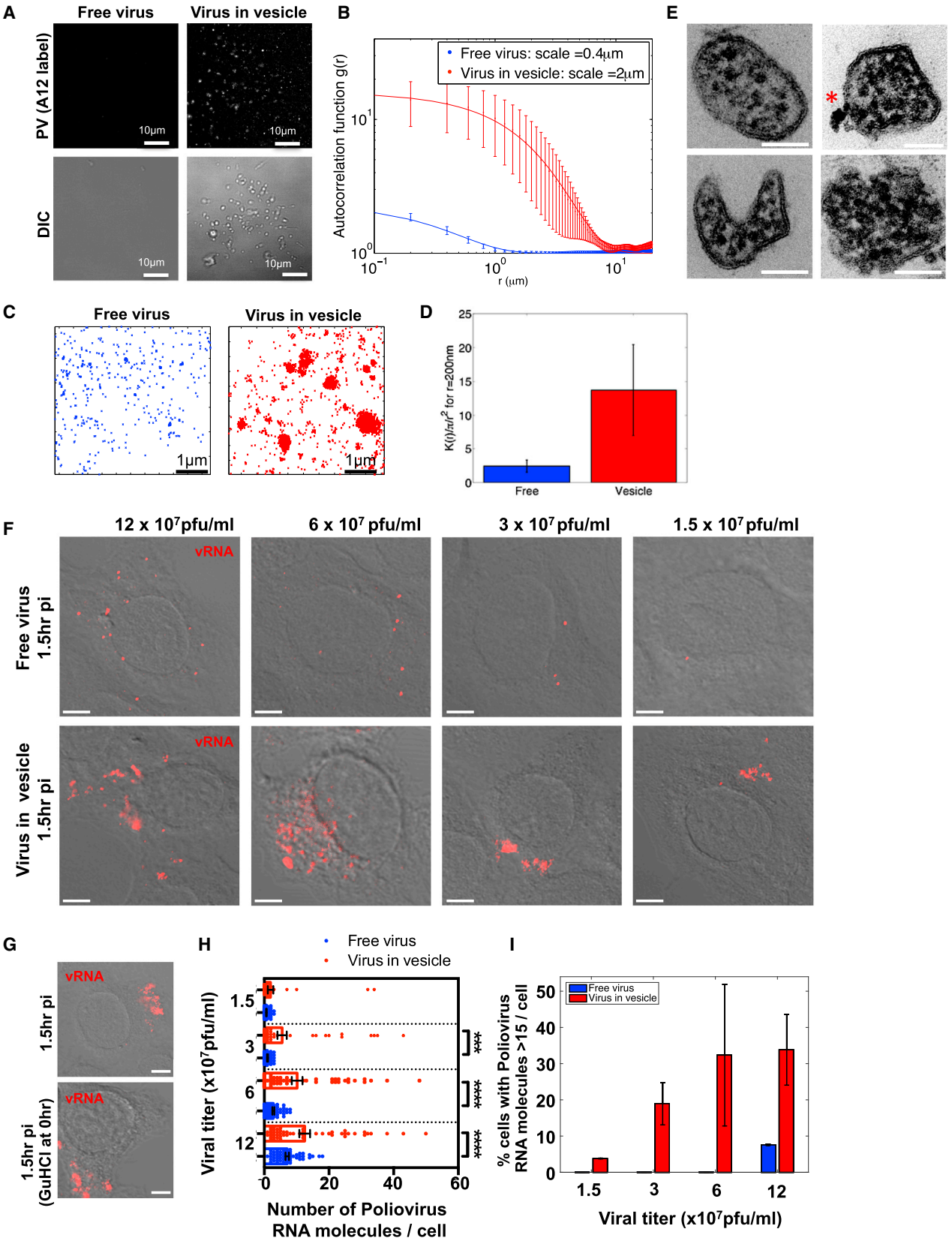

(legend on next page)

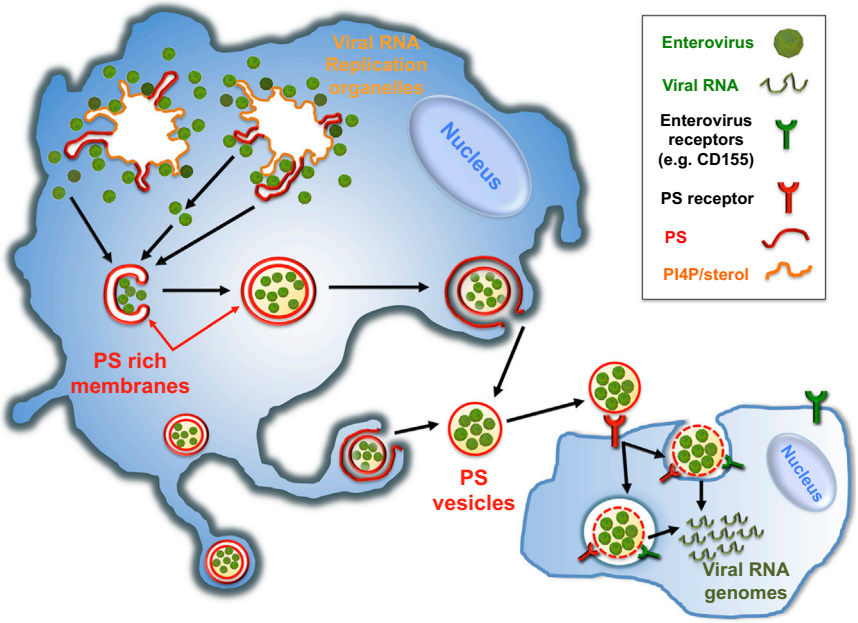

Figure 6. Model

Assembled mature enteroviruses are released from the replication organelles into the cytoplasm. Clusters of multiple viral particles are selectively captured by double-membraned organelles that originate from the ER and ER-derived replication organelles. These double-membraned organelles, which resemble autophagosomes, contain PS lipids on both the lumenal and cytoplasmic leaflets of their membranes. They fuse with the plasma membrane and release a unilamellar PS-lipid-enriched vesicle, containing multiple viral particles, into the extracellular medium. This vesicle then facilitates infection in a PS-lipid and viral receptor-dependent mechanism resulting in the collective transfer to a new recipient host cell of multiple viral RNA genomes. This mode of viral transmission enhances infection efficiency and potentially allows for genetic complementation among quasispecies.

could be prematurely triggered by inhibiting RNA synthesis with GuHCL (Figure S1A). Enteroviral 2C proteins may modulate the close coupling between RNA synthesis kinetics and capsid release from replication organelles as 2C proteins are not only localized to the replication organelles and required for viral RNA synthesis but also physically interact with capsids (Liu et al., 2010).

Once the capsids dissociated from the replication organelles, they were sequestered within double-membraned LC3-II-positive autophagosome-like organelles. How the viral cargo is recognized and captured within these organelles, the capsid-associated determinants, and whether LC3-II proteins play a role in these processes as they do in canonical autophagy pathways (Rogov et al., 2014) is currently unknown. Interestingly, unlike canonical autophagosomes that fuse with lysosomes and degrade their cytoplasmic cargo, these capsid-containing organelles fused with the plasma membrane to non-lytically release >80% of the PV particles into the extracellular environment within unilamellar vesicles of size range 200–400 nm. Notably, the SNARE protein syntaxin 17 was not localized to the autophagosome-like organelles to regulate their fusion with lysosomes, but instead was found sequestered away at the replication organelles (Figure S1I). Whether specific enteroviral proteins actively modulate its subcellular localization or it is an indirect consequence of the affinity of the syntaxin 17 hydrophobic hairpin tail for the PI4P/cholesterol rich replication organelle membranes remains to be investigated. This type of non-conventional secretion of autophagosomal membranes from the cell has never been reported and identifying the machinery regulating this process, including determining which cytoskeletal components and SNARE proteins are utilized for movement out to the periphery and fusion with the plasma membrane, may provide novel therapeutic targets to block enterovirus release from cells.

Figure 5. PS Vesicles Contain Clustered PV Particles, which Enable Multiple Viral RNA Genomes to Be Collectively Transferred into a New Host Cell

(A) TIRF and DIC images of free and vesicle-associated PV particles labeled with Atto488-labeled A12 antibody.

(B) Difference in distribution of fluorescence in (A) by computation of the radial autocorrelation function *g(r)*.

(C) dSTORM imaging free and vesicle-associated viral particles labeled with Atto488-A12 antibody.

(D) Calculation of Ripley's *K* function to assess the degree of clustering of vesicle-associated PV particles relative to free particles. Data represented as mean ± SEM.

(E) PS vesicles isolated from PV-infected cells using Annexin V microbeads were imaged by transmission electron microscopy. Note the numerous electron-dense viral particles in each vesicle and the unilamellar surrounding membrane. Asterisk shows Annexin V microbead attached to the exterior of one vesicle. Scale bars represent 100 nm.

(F) Collected intact vesicles or free viral particles from PV-infected cells were incubated with a confluent layer of new host cells at different viral titers. Viral RNAs were monitored by single molecule RNA FISH and imaged by dual confocal/DIC microscopy at 1.5 hr p.i. Shown are images of single HeLa cells infected with either free viral particles or vesicle-associated viral particles. Images presented were acquired with the same microscopy settings. Scale bar represents 2 μm.

(G) Collected vesicles were incubated with cells with/without GuHCL for 1.5 hr and viral RNA molecules were monitored by single molecule RNA FISH (see also Figure S3 for quantification). Scale bar represents 2 μm.

(H) Quantification of the number of viral RNA molecules per cell in cells infected with either free (n = 55 cells) or vesicle-associated PV particles (n = 55 cells). ***$p < 2.10^{-3}$; ****$p < 10^{-4}$.

(I) Percent of cells with 15 or greater PV RNA puncta was quantified for cells infected with either free or vesicle-associated PV particles for each viral titer shown. Data represented as mean ± SEM.

PS vesicles non-lytically released from cells were selectively enriched in mature enteroviral particles (Figure 3). While we cannot exclude the possibility that non-PS vesicles may also contribute to the non-lytic release of enteroviral particles, the observed significant inhibition of subsequent infection when PS is blocked (Figures 4C and 4D) suggest that PS vesicles constitute a large fraction of the non-lytic conduit for enteroviral release from cells. Live-cell time-lapse imaging in the presence of fluorescently labeled Annexin V protein revealed that the outer membrane leaflet of the released vesicle and hence topologically equivalent to the lumenal membrane leaflet of the double membraned organelle pre-fusion, contained PS lipids (Figures 3A–3D; Movie S1). The ER and/or the ER-derived replication organelles both have PS lipids on their lumenal and cytoplasmic leaflets (Leventis and Grinstein, 2010; Lev, 2012) (Figure 1D), and moreover, the PS can flip between these two leaflets (Clark, 2011). Thus it is likely that the host source for the autophagosome-like organelles is the ER and/or ER-derived replication organelles. Supporting this conclusion the released PS vesicles indeed contained ER markers including the integral ER membrane protein calnexin (Figure S2B).

Super-resolution imaging and transmission electron microscopy revealed extracellular PS vesicles to be containing multiple viral particles, at least 20 per 200 nm cross-section (Figures 5A–5E). Supporting these data, in single molecule RNA FISH experiments, we found that infection by PV particles in vesicles allowed the collective transfer of multiple viral genomes into a single host cell (Figures 5F–5I). One important implication of these findings is that it ties the fate of individual viral genomes from previous rounds of replication to each other and thereby may provide selective advantages in terms of replication kinetics and genetic diversity relative to free viral particle genomes (i.e., not in vesicle). Indeed, infection efficiency was significantly higher when cells were infected with PV particles in vesicles as opposed to an equivalent number of free virus particles (Figures 4E and 4F). Enteroviruses as well as all other positive-stranded RNA viruses, are enormously diverse in genomic variety due to the inherent error rates and lack of proof reading in their RNA polymerases that can generate large numbers of viral quasispecies after even a single round of infection (Bordería et al., 2011). Vesicular transfer of multiple particles among cells would increase the chances of genetic complementation among viral quasispecies, potentially benefiting the replication efficiency of otherwise attenuated or weak genomes and enabling them to maintain a presence in the genetic pool. Indeed our findings may provide a cellular mechanism to explain the results of Vignuzzi et al. (2006) where cooperative interactions between neurotropic and non-neurotropic PV quasispecies were reported. Second, when multiple viral genomes are transferred to a single cell, the likelihood of one or more genomes surviving the hostile host environment to override host defenses and replicate may be higher. Third, for positive-stranded RNA viruses, rather than a single genome having to switch between RNA translation and RNA synthesis activities (until sufficient levels of viral RNA have been synthesized to partition those functions among genomes), multiple genomes could right from the start of infection partition RNA translation and RNA synthesis functions among themselves and enhance overall replication kinetics and viral protein levels. Finally the PS lipids on the vesicles themselves could enhance infection efficiency by attracting PS scavenging cells, such as macrophages and dendritic cells, to take up the viral genomes and provide a host environment for replication. In particular, we found that PV particles within vesicles could replicate significantly more efficiently within primary macrophages than free PV particles (Figure 4F).

What is the mechanism whereby viral particles within vesicles infect host cells? We found infection to be dependent not only on the virus-specific receptor expressed by the host but also on the PS lipids associated with the vesicle having access to the host cell (Figures 4C and 4D). One potential mechanism to explain these findings is that PS lipids on vesicles engage PS receptors on the recipient host cell prior to the viral particles engaging their own receptors. The binding to PS receptors can trigger phagocytic uptake of vesicles (Hoffmann et al., 2001) followed by lysis or permeabilization of the vesicle within the endosomal compartment to then enable viral particles to engage their specific receptors (Figure 6). Equally possible, binding to PS receptors may lead to permeabilization of the vesicle on the cell surface, resulting in the release of a concentrated bolus of viral particles in the immediate vicinity of the cell. The latter mechanism may also provide access to neutralizing antibodies which bind capsids and block infection. Reliance on PS lipids and PS receptors for infection has been documented for a number of other viruses including vaccinia, Dengue, Ebola, hepatitis A virus, and HIV (Sui et al., 2006; Mercer and Helenius, 2009; Feng et al., 2014; Morizano and Chen, 2014). The specific use of PS lipids by enteroviruses as well as other viruses to traffic between cells may have significant in vivo implications for viral pathogenesis and tissue tropism. In particular, the infection of primary macrophages, the major PS sensing cells in the body, may provide enteroviruses with the ability to target a key cell subset of the immune system while suppressing its inflammatory responses, as PS lipids have been well documented to inhibit inflammatory cytokine production by macrophages (Hochreiter-Hufford and Ravichandran, 2013). PS-lipid vesicles may also help enteroviruses exploit the natural motility of macrophages and help spread them distant sites including perhaps the CNS (Ousman and Kubes, 2012).

In summary, we report here a novel mode of viral transmission among cells where multiple viral particles are clustered and collectively released within PS-lipid-enriched vesicles. This provides greater infection efficiency and potentially an opportunity for cooperation and complementation among viral quasispecies. This mode of transmission links the fate of multiple viral particles to one another and may have implications for maintaining viral genetic diversity within viral evolution.

EXPERIMENTAL PROCEDURES

All detailed protocols and information regarding plasmids, antibodies, cell culture, virus infection, and propagation are provided in the Extended Experimental Procedures.

Immunofluorescence

Cells were plated on glass coverslips and fixed with 4% PFA for 15 min at RT. Cells were permeabilized with either 0.2% Saponin or 0.1% Triton X-100 and sequentially incubated with primary and fluorophore-tagged secondary

antibodies. Coverslips were mounted in Fluoromount-G (Southern Biotech) and imaged.

Confocal Microscopy

All confocal images were obtained with an LSM780 laser scanning confocal microscope system (Carl Zeiss) and images were analyzed with either Zen (Carl Zeiss) or Image J (NIH) software.

dSTORM

Free PV particles and PV particles in vesicles were plated on gridded glass bottom dishes and fixed with 4% PFA for 15 min at room temperature. Subsequently they were permeabilized with 0.2% saponin and incubated with Atto488-conjugated A12 antibodies. An oxygen-scavenging PBS solution (10 mM NaCl, 0.5 mg/ml glucose oxidase, 40 g/ml catalase, 2% glucose, and 10 mM MEA) was used for imaging. dSTORM images were obtained on a Zeiss ELYRA PS.1 system (Carl Zeiss). Images were acquired with a Plan-Apochromat 100×/1.46 oil immersion objective and an Andor iXon 885 EMCCD camera. A total of 20,000 images were acquired per sample with an exposure time of 33 ms. Raw images were reconstructed and analyzed with ZEN software (Carl Zeiss) and MATLAB (MathWorks) using methodology from Veatch et al. (2012) and Termini et al. (2014).

Structured Illumination Microscopy

Super-resolution 3D-structured illumination microscopy (SIM) imaging was performed on a Zeiss ELYRA PS.1 system (Carl Zeiss). Images were acquired with a Plan-Apochromat 63×/1.40 oil immersion objective and an Andor iXon 885 EMCCD camera. Fifteen images per plane (five phases, three rotations) and 0.125 mm z section of 3 mm height were required for generating super resolution images. Raw images were reconstructed and processed to demonstrate structure with greater resolution by the ZEN 2011 software (Carl Zeiss).

Single Molecule RNA FISH

We performed single molecule RNA FISH according to Shaffer et al. (2013). Cells were incubated with either free or vesicle-associated PV particles for 1.5 hr. Cells were subsequently fixed in pre-chilled methanol (−20°C) for 10 min. The methanol was removed and the cells were hybridized with 10 μl of hybridization buffer containing 4 μM PV probe, 10% formamide, 2× SSC, and 10% dextran sulfate for 10 min at 37°C. Next, the samples were washed three times with pre-warmed wash buffer (10% formamide and 2× SSC) at 37°C for 1 min and imaged with Zeiss LSM780 confocal microscope.

Annexin V Labeling

Cells for live imaging were grown on coverslip-bottomed Lab-Tek chambers (Thermo Fisher) and infected with PV for 7 hr. Cells were then replaced in imaging media (DMEM Phenol Red free supplemented with 10% FBS and 50 mM HEPES [pH 7.3]). Alexa 568-Annexin V was added on the cells and imaging was performed on a Zeiss LSM780 Confocal Laser Scanning microscope (Carl Zeiss) equipped with 458 nm, 488 nm, 514 nm, 565 nm, and 633 nm laser lines and detecting system for fluorescence and DIC imaging. The microscope was additionally equipped with a heating stage and incubator with temperature, humidity, and CO_2 control for live-cell imaging.

SUPPLEMENTAL INFORMATION

Supplemental Information includes Extended Experimental Procedures, three figures, and one movie and can be found with this article online at http://dx.doi.org/10.1016/j.cell.2015.01.032.

ACKNOWLEDGMENTS

The authors would like to thank Yasmine Belkaid, Konstantin Chumakov, Ana Maria Cuervo, James Hogle, Gerald Feldman, Jennifer Jones, Jennifer Lippincott-Schwartz, Sanford Simon, Radek Dobrowolski, Wilma Friedman, Ellie Ehrenfeld and members of the Altan-Bonnet lab for fruitful discussions. The authors would like to especially thank Wen-Chin Tseng for help in constructing the graphical cartoons. The authors also thank Frank Macaluso and Geoffrey Perumal of the Albert Einstein College of Medicine Analytical Imaging facility for technical support. A.C., P.T., and C.P. were supported by grant AI091985-01A1; G.A.B. was supported by grant AI083408; H.M., P.J., and E.W. were supported by grant AI15122; and Y.C., W.D., M.H., C.B., P.C., E.S., and N.A.B. were supported by intramural NIH funds.

Received: October 2, 2014
Revised: December 13, 2014
Accepted: January 12, 2015
Published: February 12, 2015

REFERENCES

Baddeley, D., Jayasinghe, I.D., Cremer, C., Cannell, M.B., and Soeller, C. (2009). Light-induced dark states of organic fluochromes enable 30 nm resolution imaging in standard media. Biophys. J. *96*, L22–L24.

Barton, D.J., and Flanegan, J.B. (1997). Synchronous replication of poliovirus RNA: initiation of negative-strand RNA synthesis requires the guanidine-inhibited activity of protein 2C. J. Virol. *71*, 8482–8489.

Bates, M., Huang, B., Dempsey, G.T., and Zhuang, X. (2007). Multicolor super-resolution imaging with photo-switchable fluorescent probes. Science *317*, 1749–1753.

Bird, S.W., Maynard, N.D., Covert, M.W., and Kirkegaard, K. (2014). Nonlytic viral spread enhanced by autophagy components. Proc. Natl. Acad. Sci. USA *111*, 13081–13086.

Bordería, A.V., Stapleford, K.A., and Vignuzzi, M. (2011). RNA virus population diversity: implications for inter-species transmission. Curr. Opin. Virol. *1*, 643–648.

Brandenburg, B., and Zhuang, X. (2007). Virus trafficking - learning from single-virus tracking. Nat. Rev. Microbiol. *5*, 197–208.

Brandenburg, B., Lee, L.Y., Lakadamyali, M., Rust, M.J., Zhuang, X., and Hogle, J.M. (2007). Imaging poliovirus entry in live cells. PLoS Biol. *5*, e183.

Chen, Z., Chumakov, K., Dragunsky, E., Kouiavskaia, D., Makiya, M., Neverov, A., Rezapkin, G., Sebrell, A., and Purcell, R. (2011). Chimpanzee-human monoclonal antibodies for treatment of chronic poliovirus excretors and emergency postexposure prophylaxis. J. Virol. *85*, 4354–4362.

Chen, Z., Fischer, E.R., Kouiavskaia, D., Hansen, B.T., Ludtke, S.J., Bidzhieva, B., Makiya, M., Agulto, L., Purcell, R.H., and Chumakov, K. (2013). Cross-neutralizing human anti-poliovirus antibodies bind the recognition site for cellular receptor. Proc. Natl. Acad. Sci. USA *110*, 20242–20247.

Clark, M.R. (2011). Flippin' lipids. Nat. Immunol. *12*, 373–375.

Dempsey, G.T., Vaughan, J.C., Chen, K.H., Bates, M., and Zhuang, X. (2011). Evaluation of fluorophores for optimal performance in localization-based super-resolution imaging. Nat. Methods *8*, 1027–1036.

den Boon, J.A., and Ahlquist, P. (2010). Organelle-like membrane compartmentalization of positive-strand RNA virus replication factories. Annu. Rev. Microbiol. *64*, 241–256.

Doceul, V., Hollinshead, M., van der Linden, L., and Smith, G.L. (2010). Repulsion of superinfecting virions: a mechanism for rapid virus spread. Science *327*, 873–876.

Ehrenfeld, E., Maizel, J.V., and Summers, D.F. (1970). Soluble RNA polymerase complex from poliovirus-infected HeLa cells. Virology *40*, 840–846.

Fadok, V.A., Voelker, D.R., Campbell, P.A., Cohen, J.J., Bratton, D.L., and Henson, P.M. (1992). Exposure of phosphatidylserine on the surface of apoptotic lymphocytes triggers specific recognition and removal by macrophages. J. Immunol. *148*, 2207–2216.

Feng, Z., Hensley, L., McKnight, K.L., Hu, F., Madden, V., Ping, L., Jeong, S.H., Walker, C., Lanford, R.E., and Lemon, S.M. (2013). A pathogenic picornavirus acquires an envelope by hijacking cellular membranes. Nature *496*, 367–371.

Feng, Z., Li, Y., McKnight, K.L., Hensley, L., Lanford, R.E., Walker, C.M., and Lemon, S.M. (2014). Human pDCs preferentially sense enveloped hepatitis A virions. J. Clin. Invest. *125*, 169–176.

Flint, S.J., Enquist, L.W., Racaniello, V.R., and Skalka, A.M. (2009). Principles of Virology, Third Edition (ASM Press).

Hamasaki, M., Furuta, N., Matsuda, A., Nezu, A., Yamamoto, A., Fujita, N., Oomori, H., Noda, T., Haraguchi, T., Hiraoka, Y., et al. (2013). Autophagosomes form at ER-mitochondria contact sites. Nature *495*, 389–393.

Hochreiter-Hufford, A., and Ravichandran, K.S. (2013). Clearing the dead: apoptotic cell sensing, recognition, engulfment, and digestion. Cold Spring Harb. Perspect. Biol. *5*, a008748.

Hoffmann, P.R., deCathelineau, A.M., Ogden, C.A., Leverrier, Y., Bratton, D.L., Daleke, D.L., Ridley, A.J., Fadok, V.A., and Henson, P.M. (2001). Phosphatidylserine (PS) induces PS receptor-mediated macropinocytosis and promotes clearance of apoptotic cells. J. Cell Biol. *155*, 649–659.

Hsu, N.Y., Ilnytska, O., Belov, G., Santiana, M., Chen, Y.H., Takvorian, P.M., Pau, C., van der Schaar, H., Kaushik-Basu, N., Balla, T., et al. (2010). Viral reorganization of the secretory pathway generates distinct organelles for RNA replication. Cell *141*, 799–811.

Ilnytska, O., Santiana, M., Hsu, N.Y., Du, W.L., Chen, Y.H., Viktorova, E.G., Belov, G., Brinker, A., Storch, J., Moore, C., et al. (2013). Enteroviruses harness the cellular endocytic machinery to remodel the host cell cholesterol landscape for effective viral replication. Cell Host Microbe *14*, 281–293.

Itakura, E., Kishi-Itakura, C., and Mizushima, N. (2012). The hairpin-type tail-anchored SNARE syntaxin 17 targets to autophagosomes for fusion with endosomes/lysosomes. Cell *151*, 1256–1269.

Jackson, W.T., Giddings, T.H., Jr., Taylor, M.P., Mulinyawe, S., Rabinovitch, M., Kopito, R.R., and Kirkegaard, K. (2005). Subversion of cellular autophagosomal machinery by RNA viruses. PLoS Biol. *3*, e156.

Kay, J.G., Koivusalo, M., Ma, X., Wohland, T., and Grinstein, S. (2012). Phosphatidylserine dynamics in cellular membranes. Mol. Biol. Cell *23*, 2198–2212.

Kirkegaard, K., and Jackson, W.T. (2005). Topology of double-membraned vesicles and the opportunity for non-lytic release of cytoplasm. Autophagy *1*, 182–184.

Koopman, G., Reutelingsperger, C.P., Kuijten, G.A., Keehnen, R.M., Pals, S.T., and van Oers, M.H. (1994). Annexin V for flow cytometric detection of phosphatidylserine expression on B cells undergoing apoptosis. Blood *84*, 1415–1420.

Lev, S. (2012). Non-vesicular lipid transfer from the ER. Cold Spring Harb. Perspect. Biol. *4*, 1–17.

Leventis, P.A., and Grinstein, S. (2010). The distribution and function of phosphatidylserine in cellular membranes. Annu. Rev. Biophys. *39*, 407–427.

Liu, Y., Wang, C., Mueller, S., Paul, A.V., Wimmer, E., and Jiang, P. (2010). Direct interaction between two viral proteins, the nonstructural protein 2C and the capsid protein VP3, is required for enterovirus morphogenesis. PLoS Pathog. *6*, e1001066.

Lubeck, E., and Cai, L. (2012). Single-cell systems biology by super-resolution imaging and combinatorial labeling. Nat. Methods *9*, 743–748.

Mercer, J., and Helenius, A. (2009). Virus entry by macropinocytosis. Nat. Cell Biol. *11*, 510–520.

Morizano, K., and Chen, I.S. (2014). Role of phosphatidlyserine receptors in enveloped virus infection. J. Virol. *88*, 4275–4290.

Nchoutmboube, J.A., Viktorova, E.G., Scott, A.J., Ford, L.A., Pei, Z., Watkins, P.A., Ernst, R.K., and Belov, G.A. (2013). Increased long chain acyl-Coa synthetase activity and fatty acid import is linked to membrane synthesis for development of picornavirus replication organelles. PLoS Pathog. *9*, e1003401.

Ousman, S.S., and Kubes, P. (2012). Immune surveillance in the central nervous system. Nat. Neurosci. *15*, 1096–1101.

Owens, R.J., Limn, C., and Roy, P. (2004). Role of an arbovirus nonstructural protein in cellular pathogenesis and virus release. J. Virol. *78*, 6649–6656.

Raj, A., van den Bogaard, P., Rifkin, S.A., van Oudenaarden, A., and Tyagi, S. (2008). Imaging individual mRNA molecules using multiple singly labeled probes. Nat. Methods *5*, 877–879.

Robinson, S.M., Tsueng, G., Sin, J., Mangale, V., Rahawi, S., McIntyre, L.L., Williams, W., Kha, N., Cruz, C., Hancock, B.M., et al. (2014). Coxsackievirus B exits the host cell in shed microvesicles displaying autophagosomal markers. PLoS Pathog. *10*, e1004045.

Rogov, V., Dötsch, V., Johansen, T., and Kirkin, V. (2014). Interactions between autophagy receptors and ubiquitin-like proteins form the molecular basis for selective autophagy. Mol. Cell *53*, 167–178.

Shaffer, S.M., Wu, M.T., Levesque, M.J., and Raj, A. (2013). Turbo FISH: a method for rapid single molecule RNA FISH. PLoS ONE *8*, e75120.

Strauss, M., Levy, H.C., Bostina, M., Filman, D.J., and Hogle, J.M. (2013). RNA transfer from poliovirus 135S particles across membranes is mediated by long umbilical connectors. J. Virol. *87*, 3903–3914.

Strazynski, M., Krämer, J., and Becker, B. (2002). Thermal inactivation of poliovirus type 1 in water, milk and yoghurt. Int. J. Food Microbiol. *74*, 73–78.

Sui, L., Zhang, W., Chen, Y., Zheng, Y., Wan, T., Zhang, W., Yang, Y., Fang, G., Mao, J., and Cao, X. (2006). Human membrane protein Tim-3 facilitates hepatitis A virus entry into target cells. Int. J. Mol. Med. *17*, 1093–1099.

Swairjo, M.A., Concha, N.O., Kaetzel, M.A., Dedman, J.R., and Seaton, B.A. (1995). Ca(2+)-bridging mechanism and phospholipid head group recognition in the membrane-binding protein annexin V. Nat. Struct. Biol. *2*, 968–974.

Takahashi, M., Yamada, K., Hoshino, Y., Takahashi, H., Ichiyama, K., Tanaka, T., and Okamoto, H. (2008). Monoclonal antibodies raised against the ORF3 protein of hepatitis E virus (HEV) can capture HEV particles in culture supernatant and serum but not those in feces. Arch. Virol. *153*, 1703–1713.

Taylor, M.P., Burgon, T.B., Kirkegaard, K., and Jackson, W.T. (2009). Role of microtubules in extracellular release of poliovirus. J. Virol. *83*, 6599–6609.

Termini, C.M., Cotter, M.L., Marjon, K.D., Buranda, T., Lidke, K.A., and Gillette, J.M. (2014). The membrane scaffold CD82 regulates cell adhesion by altering α4 integrin stability and molecular density. Mol. Biol. Cell *25*, 1560–1573.

Veatch, S.L., Machta, B.B., Shelby, S.A., Chiang, E.N., Holowka, D.A., and Baird, B.A. (2012). Correlation functions quantify super-resolution images and estimate apparent clustering due to over-counting. PLoS ONE *7*, e31457.

Vignuzzi, M., Stone, J.K., Arnold, J.J., Cameron, C.E., and Andino, R. (2006). Quasispecies diversity determines pathogenesis through cooperative interactions in a viral population. Nature *439*, 344–348.